Dispersion, ionic bonding and vibrational shifts in phospho-aluminosilicate glasses

Thilo Grammes, Dominique de Ligny, Dintu Mathew, Kristin Griebenow, Franziska Scheffler, Florian Lindner, Claudia Aichele, Jan Dellith, Leo van Wüllen, Efstratios I. Kamitsos, Delia S. Brauer

Supplementary Information

Summary of infrared and Raman spectroscopy band assignments

In the IR spectra of phosphate-free glasses (Figure S2c) the maximum shifting from 982 to 1021 cm^{-1} corresponds to asymmetric Si-O stretching in Q_{Si}^4 units.[1-3] and the shoulder shifting from 1100 to 1150 cm^{-1} corresponds to a vibration of Q^4 units.[1,3] With phosphate incorporation (Figure S2a,e), this shoulder became more pronounced due to a new phosphate-related band (asymmetric P-O stretching in Q_P^2 units)[4-6] and shifted from 1130 to 1170 cm^{-1} with increasing silica content (Figure S2e).

The Raman spectra of phosphate-free glasses (Figure S2d) comprised three bands, of which one high frequency shoulder was only visible under cross-polarisation.[7] Here, the maximum shifting from 1005 to 1088 cm^{-1} was assigned to the $Q_{Si/Al}^{4,low}$ mode and the hidden high frequency shoulder to the $Q_{Si/Al}^{4,high}$ mode (individual bands are indicated in Figure S3). The two modes correspond to stretching of tetrahedral units with smaller ($Q_{Si/Al}^{4,low}$) and larger ($Q_{Si/Al}^{4,high}$) inter-tetrahedral bond angles.[8-15] A shoulder at lower frequencies, shifting from 970 to 1000 cm^{-1}, became visible with increasing silica content, and was assigned to the T_{2s} mode of Q^4 units (two oxygens moving towards the tetrahedral centre while the other two move away from it).[9-13]

After phosphate incorporation, the Raman spectra were dominated by two new features. A new maximum shifted from 1056 to 1068 cm^{-1} with increasing P_2O_5 content (Figure S2b) and from 1050 to 1076 cm^{-1} with increasing SiO_2 content (Figure S2f). A new high frequency shoulder shifted from 1200 to 1215 cm^{-1} with increasing P_2O_5 content (Figure S2b) and from 1195 to 1210 cm^{-1} with increasing SiO_2 content (Figure S2f). The phosphate-related maximum was assigned to the symmetric stretching and the shoulder to asymmetric stretching of Q_P^2 units.[4-6,16-18] Both phosphate-related Raman bands were additionally assigned to Al-O-P bonds,[19-22] thus supporting the interpretation of the refractive index trend with increasing phosphate content as being partially caused by Al-O-P bonds.

Dispersion formula from refractive index fitting

The dispersion fits were done with a two-term Sellmeier approximation, which already yielded very goot fits to the data (see below). A third term in the Sellmeier fit could not be added since more investigated wavelengths would have been required.

The goodness of the Sellmeier fit is confirmed by high coefficients of determination (R^2>0.98 for all glasses, see Suppl. Table S1). To provide an additional measure of the accuracy of refractive indices calculated from the Sellmeier fit, we determined the standard deviation σ of the fit as the square root of the Bessel-corrected unbiased sample variance (all values < $9e^{-4}$; see Suppl. Table S1).

$$\sigma = \sqrt{\sum_{i=1}^{k} \frac{\left(n_{measured} - n_{fitted}\right)^2}{k-1}} \qquad \text{(S1)}$$

Here, k is the number of investigated wavelengths.

Supplementary Figures

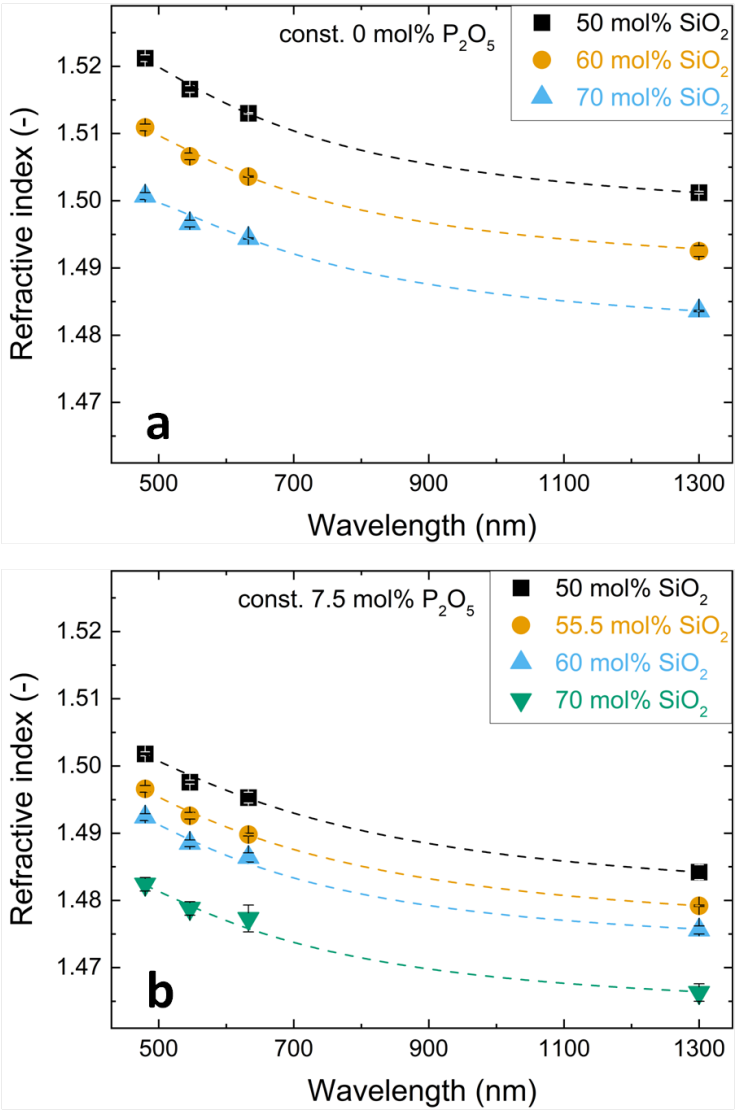

Figure S1. *Changes in refractive index with wavelength for the glass series with increasing silica content and (a) constant 0 mol% P_2O_5 or (b) constant 7.5 mol% P_2O_5. Dashed lines are fits with a two-term Sellmeier approximation (details in Suppl. Table S1).*

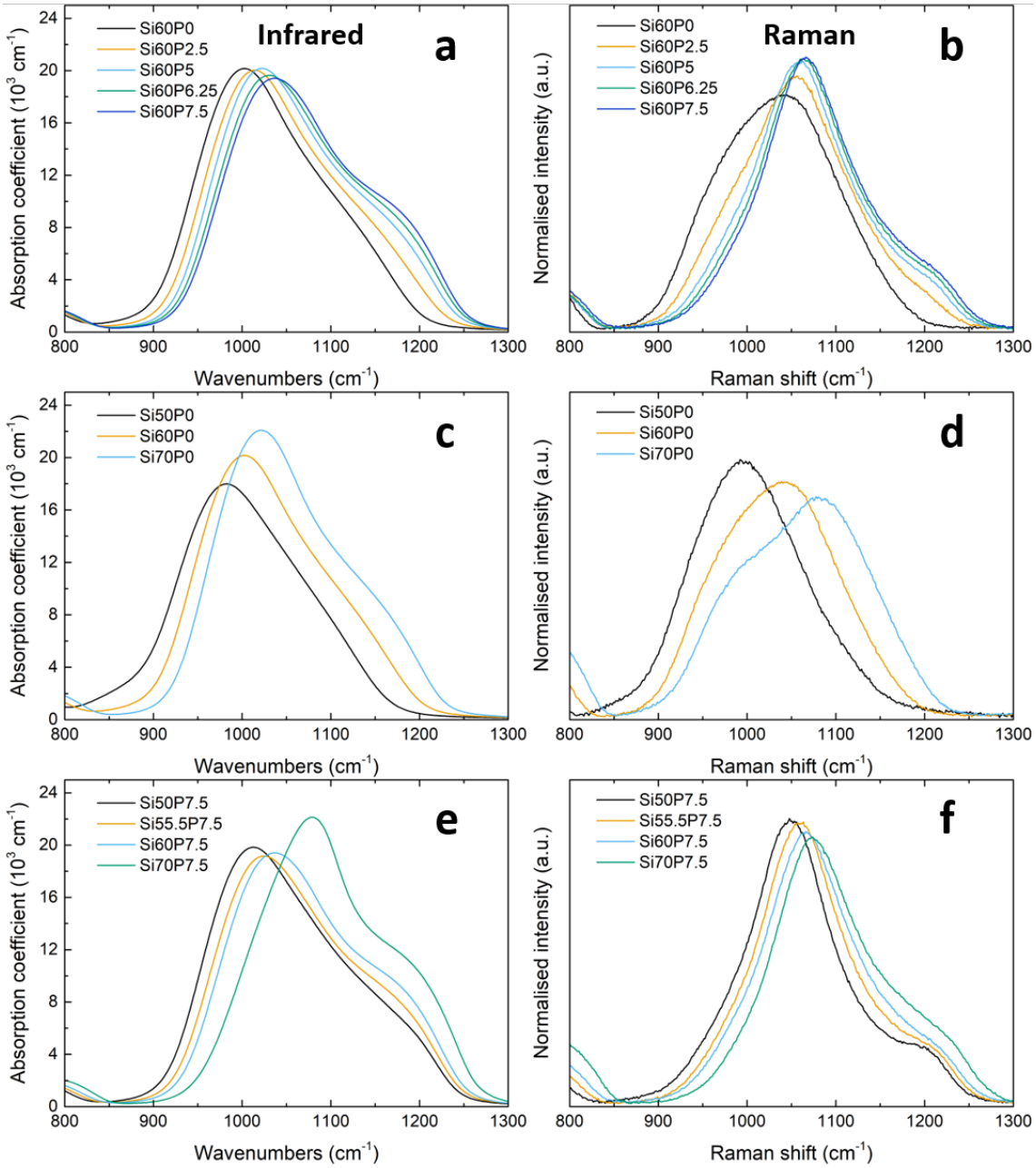

Figure S2. *High frequency envelope of the IR (left) and Raman spectra (right) for the three glass series with (a,b) increasing P_2O_5 content (constant 60 mol% SiO_2), (c,d) with increasing SiO_2 content and constant P_2O_5 contents of 0 mol% or (e,f) 7.5 mol%. A shift of the envelope to higher wavenumbers occurred in all series. For details see text.*

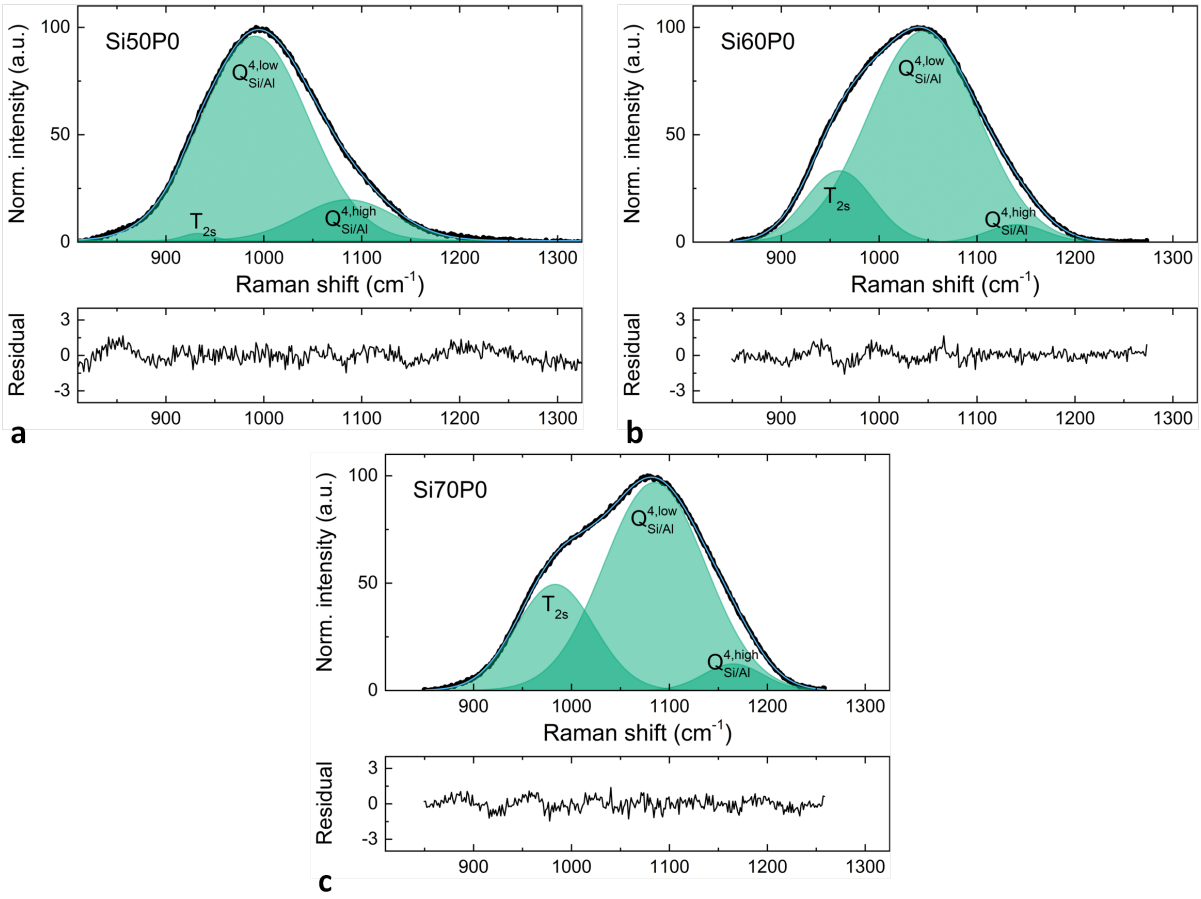

Figure S3. *Deconvoluted high frequency Raman spectra and residuals for the phosphate-free glasses (a) Si50P0, (b) Si60P0 and (c) Si70P0. Experimental data are presented in black, deconvoluted bands in green and the sum curve of the fitted model in blue.*

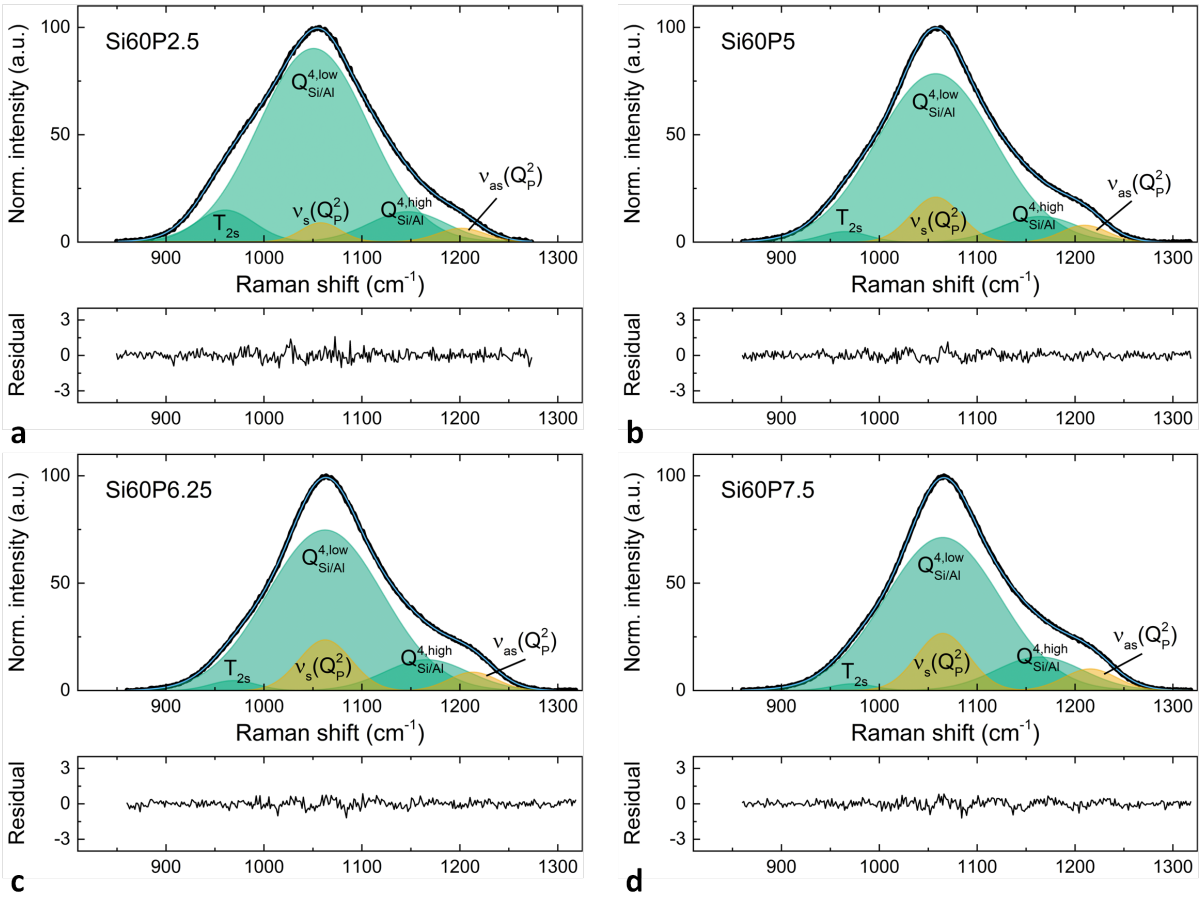

Figure S4. *Deconvoluted high frequency Raman spectra and residuals for the phosphate-containing glasses (a) Si60P2.5, (b) Si60P5, (c) Si60P6.25 and (d) Si60P7.5. Experimental data are presented in black, deconvoluted bands in green and orange and the sum curve of the fitted model in blue.*

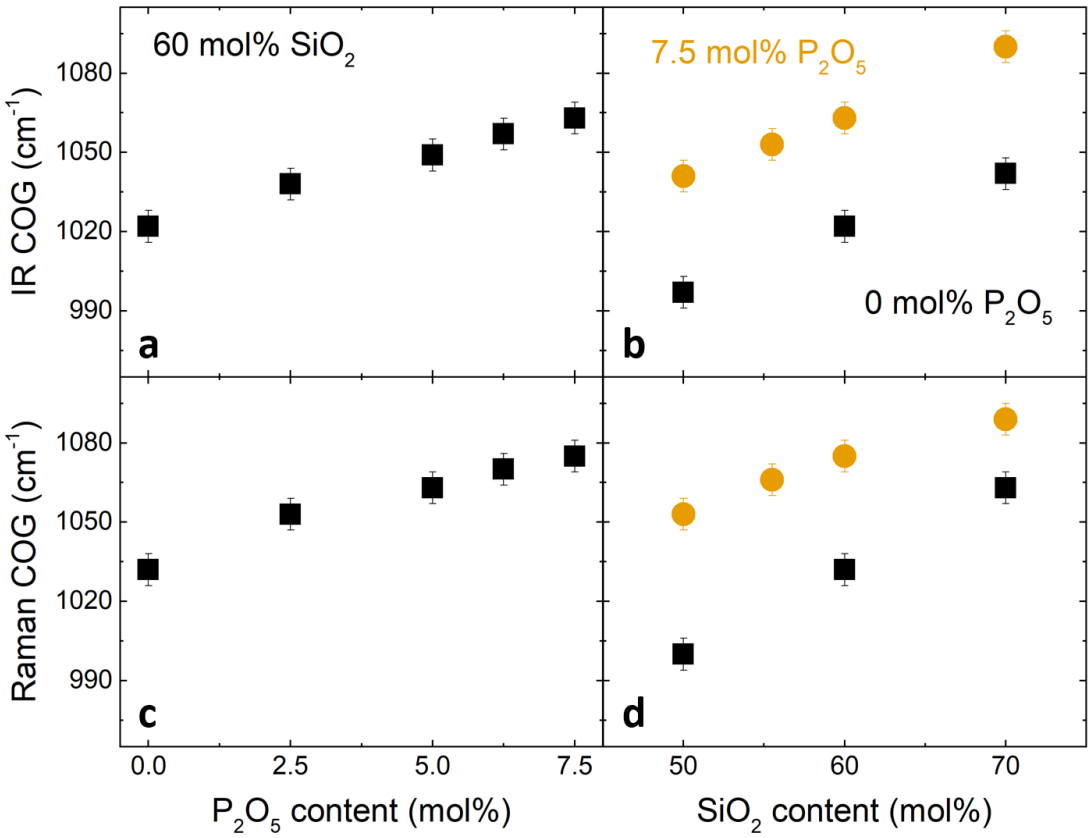

Figure S5. *Changes in the centre of gravity (COG) of the high frequency envelope of the IR (a,b) and Raman spectra (c,d) with (a,c) increasing P_2O_5 content and constant 60 mol% SiO_2 and with (b,d) increasing SiO_2 content and constant P_2O_5 contents of 0 mol% (black squares) or 7.5 mol% (orange circles).*

Supplementary Tables

Table S1. Fitting results of a two-term Sellmeier approximation for the dispersion of the studied glasses and Abbe numbers.

Series	Glass	B_1	C_1	B_2	C_2	R^2	Standard deviation of fit	Abbe number v_e
Series i	Si60P0	-96.77284	41987.96731	97.99026	41662.52717	0.99561	5.21E-04	65.3983
	Si60P2.5	-128.02863	39372.20971	129.22496	39153.10215	0.99992	7.34E-05	58.06158
	Si60P5	-144.14989	39419.6307	145.33345	39220.24242	0.99776	3.54E-04	64.59081
	Si60P6.25	-127.82644	41124.75418	129.00052	40891.05941	0.99595	4.72E-04	65.41014
	Si60P7.5	-78.39322	39315.03854	79.56104	38953.18424	0.99234	6.29E-04	66.84926
Series ii	Si50P0	-86.81553	43142.92958	88.05699	42772.27966	0.99787	3.95E-04	59.46718
	Si60P0	-96.77284	41987.96731	97.99026	41662.52717	0.99561	5.21E-04	65.3983
	Si70P0	-110.08837	45860.55428	111.27796	45548.92397	0.98921	7.58E-04	73.61894
Series iii	Si50P7.5	-116.60929	-30668.19522	117.79875	-30153.75974	0.99359	6.02E-04	71.04377
	Si55.5P7.5	-85.30115	-27779.19186	86.47678	-27145.05736	0.99754	3.69E-04	67.93973
	Si60P7.5	-78.39322	39315.03854	79.56104	38953.18424	0.99234	6.29E-04	66.84926
	Si70P7.5	-57.507	39128.27412	58.64782	38647.64685	0.98318	9.00E-04	68.81379

Table S2. Overview of electronic polarisability, α_m (Å^3), oxygen polarisability, α_{O2-} (Å^3), theoretical (and experimental) optical basicity, Λ_{th} and Λ_{exp}, and the centre of gravity (COG) of the high frequency envelope of IR and Raman spectra (cm^{-1}).

Series	Glass	α_m	α_{O2-}	Λ_{th} (Λ_{exp})	IR COG	Raman COG
Series i (Pb)	Si60P0	3.272 ± 0.013	1.580 ± 0.007	0.58 (0.57)	1022 ± 6	1032 ± 6
	Si60P2.5	3.346 ± 0.014	1.561 ± 0.007	0.56	1038 ± 6	1053 ± 6
	Si60P5	3.417 ± 0.014	1.541 ± 0.007	0.55 (0.54)	1049 ± 6	1063 ± 6
	Si60P6.25	3.450 ± 0.014	1.531 ± 0.007	0.54	1057 ± 6	1070 ± 6
	Si60P7.5	3.497 ± 0.015	1.528 ± 0.007	0.53 (0.52)	1063 ± 6	1075 ± 6
Series ii	Si50P0	3.385 ± 0.014	1.627 ± 0.007	0.61	997 ± 6	1000 ± 6
	Si60P0	3.272 ± 0.013	1.580 ± 0.007	0.58	1022 ± 6	1032 ± 6
	Si70P0	3.192 ± 0.013	1.550 ± 0.007	0.56	1042 ± 6	1063 ± 6
Series iii	Si50P7.5	3.572 ± 0.015	1.553 ± 0.007	0.55	1041 ± 6	1053 ± 6
	Si55.5P7.5	3.522 ± 0.015	1.535 ± 0.007	0.54	1053 ± 6	1066 ± 6
	Si60P7.5	3.497 ± 0.015	1.528 ± 0.007	0.53	1063 ± 6	1075 ± 6
	Si70P7.5	3.425 ± 0.016	1.504 ± 0.007	0.51	1090 ± 6	1089 ± 6

Errors for optical basicity are estimated to be about 0.01.

Table S3. Overview of IR and Raman spectroscopy band assignments. Band positions (in wavenumbers) are given for each of the three glass series (with constant 60 mol% SiO_2, constant 0 mol% P_2O_5 and constant 7.5 mol% P_2O_5, respectively).

Wavenumber range (cm^{-1})			Assignments
Series i	***Series ii***	***Series iii***	
60 mol% SiO_2	0 mol% P_2O_5	7.5 mol% P_2O_5	
	Infrared		
1003-1037	982-1021	1013-1079	Q_{Si}^4 asymmetric stretching [1-3,23]
1100-n.d.¶*	1100-1150*	n.d.	Q^4 units [1,3]
1170*	-	1170*	Asymmetric P-O stretching in Q_P^2 units [4-6]
	Raman		
985-1027††,†	970-1000†	n.d.	T_{2s} tetrahedral mode‡ [9-13]
1048-n.d.	1005-1088	n.d.	$Q_{Si/Al}^{4,low}$ tetrahedral mode‡‡ [9-13]
1056-1068	-	1050-1076	Q_P^2 symmetric stretching [4-6,16-18]
			Al-O-P bonds [19-22]
1070-n.d.*†	1040-1090*†	n.d.	$Q_{Si/Al}^{4,high}$ tetrahedral mode‡‡ [9-13]
1200-1215*	-	1195-1210*	Q_P^2 asymmetric stretching [4-6,16-18]
			Al-O-P bonds [19-22]

* Larger uncertainty of band position (±20 cm^{-1}) because only shoulders are available for determination.

¶ n.d.: Not distinguishable because band was hidden under phosphate-related bands.

† Position determined from VH Raman spectra.

†† Position determined from spectra measured at 514 nm excitation instead of 488 nm. At 488 nm the band was not clearly distinguishable because of luminescence.

‡ Stretching of TO_4 tetrahedra with two O moving towards T and the other two O moving away from it.

‡‡ Stretching of $Q_{Si/Al}^4$ units with larger ($Q_{Si/Al}^{4,high}$) or smaller ($Q_{Si/Al}^{4,low}$) intertetrahedral angles.

References cited in supplement

1. M. D. Ingram, J. E. Davidson, A. M. Coats, E. I. Kamitsos and J. A. Kapoutsis, *Glastechnische Berichte - Glass Science and Technology*, 2000, **73**, 89-104.
2. E. I. Kamitsos, A. P. Patsis and G. Kordas, *Physical Review B*, 1993, **48**, 12499-12505.
3. E. Stavrou, D. Palles, E. I. Kamitsos, A. Lipovskii, D. Tagantsev, Y. Svirko and S. Honkanen, *Journal of Non-Crystalline Solids*, 2014, **401**, 232-236.
4. K. Griebenow, U. Hoppe, D. Möncke, E. I. Kamitsos and L. Wondraczek, *Journal of Non-Crystalline Solids*, 2017, **460**, 136-145.
5. I. Konidakis, C. P. E. Varsamis, E. I. Kamitsos, D. Möncke and D. Ehrt, *Journal of Physical Chemistry C*, 2010, **114**, 9125-9138.
6. L. L. Velli, C. P. E. Varsamis, E. I. Kamitsos, D. Möncke and D. Ehrt, *Physics and Chemistry of Glasses*, 2005, **46**, 178-181.
7. T. Grammes, D. de Ligny, F. Scheffler, A. Nizamutdinova, L. van Wüllen, E. I. Kamitsos, J. Massera and D. S. Brauer, *The Journal of Physical Chemistry B*, 2022, **126**, 9911−9926.
8. F. Galeener, *Physical Review B*, 1979, **19**, 4292-4297.
9. C. Le Losq and D. R. Neuville, *Chemical Geology*, 2013, **346**, 57-71.
10. P. McMillan, B. Piriou and A. Navrotsky, *Geochimica et Cosmochimica Acta*, 1982, **46**, 2021-2037.
11. D. R. Neuville, L. Cormier, V. Montouillout, P. Florian, F. Millot, J. Rifflet and D. Massiot, *American Mineralogist*, 2008, **93**, 1721-1731.
12. D. R. Neuville and B. O. Mysen, *Geochimica et Cosmochimica Acta*, 1996, **60**, 1727-1737.
13. A. N. Novikov, D. R. Neuville, L. Hennet, Y. Gueguen, D. Thiaudiere, T. Charpentier and P. Florian, *Chemical Geology*, 2017, **461**, 115-127.
14. F. Seifert, B. O. Mysen and D. Virgo, *American Mineralogist*, 1982, **67**, 696-717.
15. P. Sen and M. Thorpe, *Physical Review B*, 1977, **15**, 4030-4038.
16. R. Brow, D. Tallant, S. Myers and C. Phifer, *Journal of Non-Crystalline Solids*, 1995, **191**, 45-55.
17. D. Palles, I. Konidakis, C. P. E. Varsamis and E. I. Kamitsos, *RSC Advances*, 2016, **6**, 16697-16710.
18. A. Yadav and P. Singh, *RSC Advances*, 2015, **5**, 67583-67609.
19. H. Gan and P. C. Hess, *American Mineralogist*, 1992, **77**, 495-506.
20. S. G. Kosinski, D. M. Krol, T. M. Duncan, D. C. Douglass, J. B. MacChesney and J. R. Simpson, *Journal of Non-Crystalline Solids*, 1988, **105**, 45-52.
21. B. O. Mysen, *Contributions to Mineralogy and Petrology*, 1998, **133**, 38-50.
22. B. O. Mysen, F. J. Ryerson and D. Virgo, *American mineralogist*, 1981, **66**, 106-117.
23. E. I. Kamitsos, *Physical Review B*, 1996, **53**, 14659-14662.